

An experiment and a model of the rise of a gas bubble in a liquid

Carlos Chiquete* and Sairam Rayaprolu†

The University of Arizona, Tucson, Arizona 85721

Using high speed cameras, the behavior of gas bubbles in ginger ale was recorded over an interval of time. Bubbles were observed to be nearly spherical and the velocities and the radii of the bubbles were measured over time. These quantities were noted to depend on time and on the depth of the bubble in the liquid. A model based on a classic force balance, Kelvin impulse effect, and a variable viscous drag on the bubble was considered and compared to experimental results. The results were analyzed and possible avenues for improvement are proposed.

I. Introduction

Gas bubble dynamics in liquids have been treated extensively in fluid mechanics literature.¹⁻⁵ Specifically, the problem of bubble rise has a broad application in the realm of the biochemical and polymer industries. In addition, it raises an interesting mathematical problem within the scope of the continuum equations of fluids or Navier-Stokes equations. Recently, the full Navier-Stokes equations have been solved numerically in the case of bubble-rise by Yang et al.¹ who consider differing initial shapes of the bubbles and their effect on the subsequent evolution of the bubbles. Also, much work has been done in the case of a submerged source of gas that forms bubbles at some capillary tube.^{6,7} The specific problem of time-varying radius of a bubble has been treated recently as well.⁷⁻⁹ Chaotic motion of bubbles subjected to periodic pressure gradients have been observed for some time.¹⁰

The present work deals with bubble rise in a quiescent fluid with bubbles forming from the nucleation process and not a specific submerged source. In Ref. 11, Kwak and Patton write that bubbles spontaneously form from saturated liquid-gas solutions that are rapidly decompressed. This decompression process and the subsequent behavior of the liquid-gas solution can be observed and recorded experimentally. The corresponding experiment was carried out in 2004 at the University of Arizona Applied Mathematics Laboratory. A commercial Ginger Ale beverage was poured into a $10 \times 10 \times 45$ mm vial and the release of bubbles recorded by a high-speed video camera fitted with close-up lens attachments. The cameras allowed measurement of the positions and the apparent area of the gas bubbles as they rose to the surface of the vessel. Assuming a spherical shape, the radii were computed from this data.

This experiment served as the basis for the consideration of a mathematical model for the phenomena of bubble rise in a liquid. Another phenomenon under study was the expansion of gas bubbles in a liquid. The expansion has been treated in classical fluid mechanics texts.¹² The dynamics of bubble rise have been studied extensively through the use of so-called force balance models. This was the approach that was undertaken in the present work. Theoretical studies of bubble rise consider a variety of forces that act on the bubble including: buoyancy, history (or memory) force, viscous drag, inertial force, surface tension and pressure forces.² The present work considered only the inertial, drag and buoyant forces.

The structure of this paper is as follows: a description of the phenomenon observed in the experiment is presented, the method of data acquisition is then briefly described, the data is analyzed and relevant aspects are pointed out. A theoretical model for the behavior is proposed and the numerical results of the model are compared with the relevant data extracted from the experiments. Finally, the results are discussed and summarized. Possible future directions are also presented.

*Graduate Student, Program in Applied Mathematics

†Graduate Student, Program in Applied Mathematics

II. Experiment set-up and Method of data acquisition

A. Experimental set-up

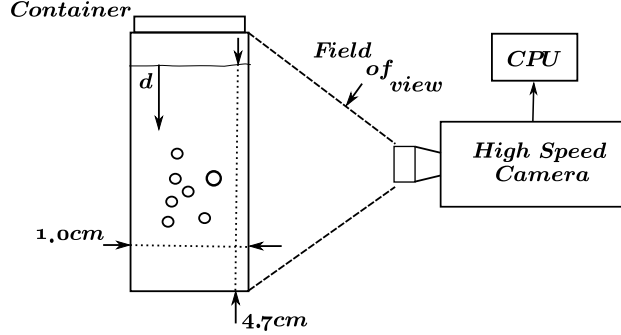


Figure 1. The experimental setup.

The experimental setup was as follows. A bottle of ginger ale was opened and subsequently poured into a small 10mm vial that was placed directly in front of a high speed video camera operating at 500 frames per second as shown in Figure 1. Four video recordings, totaling 30 seconds, taken at differing times after the initial pour were recorded and stored in a computer. Gas bubbles were observed in all four video recordings. These are summarized in Table 1. The pixel dimensions of all 4 videos were 1280×256 . A static image of the vial was taken with a ruler so as to define the scale of the video recordings. It was found to be 197.44 pixels per cm with the help of the imaging program ImageJ. This program allows analysis of sequences of images and includes extensive image analysis options. The specific procedure used to measure the relevant quantities is described in section IIB.

File	Duration	Time elapsed	Temperature of liquid
File	Duration (sec)	(minutes)	(Celsius)
1	8.188	0	16
2	7.490	50	16
3	6.809	85	24
4	8.188	155	24

Table 1. Summary of data file duration and time taken

Figure 2 shows the qualitative difference between what was observed in the files. Files 1 and 2 show the initial result of the pour and are represented by Figure 2 (a). The bubbles were attached to the wall and were many times larger than the bubbles that could be observed in motion. However, most of the large bubbles eventually moved to the surface.

The results for videos 3 and 4 are presented in Figure 2 (b). A chain of small bubbles that were translating vertically to the surface as in Figure 2 with comparable velocities were observed. These bubbles appeared to originate from a single point in the vial. Files 3 and 4 had different points of origin for the bubbles with respect to the surface, 2.20 and 4.13 cm respectively. There were no more bubbles attached to the wall. In addition the bubbles were entrained as they moved. New bubbles were continually formed at roughly the same depth.

The mechanics of the formation of large bubbles was ignored within the scope of this work. The focus of this work is on videos 3 and 4 and the chain of bubbles that form as a result of the equilibration of the fluid to atmospheric pressure.¹¹ The videos allowed easy measurement of translation and time intervals from which the velocity measurements were derived and assuming a spherical volume, the radii of said bubbles.

B. Data Acquisition Algorithm

The freeware ImageJ software has various image analysis options. In order to measure the position and radii of the bubbles the 'measure' tool included in ImageJ was utilized. The steps were as follows:

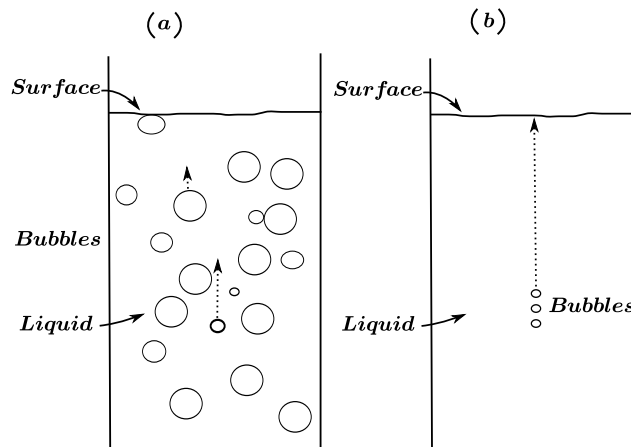


Figure 2. The motion of the bubbles is represented via the dotted lines.

1. A sequence of static images was extracted from the video files. These were loaded into the image analysis software.
2. The included 'find edges' tool was then utilized to find the boundaries of the objects in the images.
3. The 'threshold' tool was used to maximize the contrast between the bubbles and the background.
4. The 'wand' tool was used to select the various bubbles and the 'measure' tool was used to record the center-of-mass along with other relevant data. The program also systematically fitted an ellipse to the selected bubble area. The resultant semi-major and semi-minor axis measurements were used to obtain the radii.
5. This process was repeated over successive frames to obtain a displacement profile over time. The latter was used to obtain the velocities, represented by the number of intervening frames, at the various time intervals.

Since the frame rate was 500 frames per second, the interval of time between frames was .002 seconds. The data was obtained at 25 frame intervals or equivalently .05 second intervals.

III. Data

The major focus of this work involves the physical translation of the gas bubbles in the liquid. These were measured by iteratively recording the position of the center of a particular bubble through an interval of time at discrete intervals of around $\Delta t = 0.05$ seconds. The data was such that the bubble velocities were measured from differing nucleation points. The data is collected in figure 3, plotting the velocities versus depth for bubbles from videos 3 and 4. For the bubbles that began their ascent deeper in the liquid one can notice that the velocity begins to level off as time goes on and the bubble gets nearer to the free surface of the container. It is possible that the bubble was approaching a steady state. The bubbles that began rising from roughly 2 cm show an almost linear profile.

The radius of the bubbles was also measured assuming a spherical shape. It is apparent that there were two phases to the bubble expansion that can be observed from the diamond and square data: an initially large rate of change followed by an eventual moderation. This was especially apparent in the case of the square data which represented an isolated bubble in video 4. This bubble began its ascent from a greater depth than the previous bubbles. It was also not a part of the column of bubbles represented by the diamond symbols. This particular bubble can then be observed over essentially the whole length of the container and it is to be noted that it grew to a larger size as a result. Its velocity was also higher near the surface than its entrained counterparts.

The remarkable fact that is apparent from these data is that the shapes of the velocity and the radius profiles nearly coincide for bubbles starting from the same nucleation point. The data for the radius is more

variable but the trend is still clear. The mechanism that was working to increase the size and velocity of the bubbles was remarkably regular across the set of bubbles.

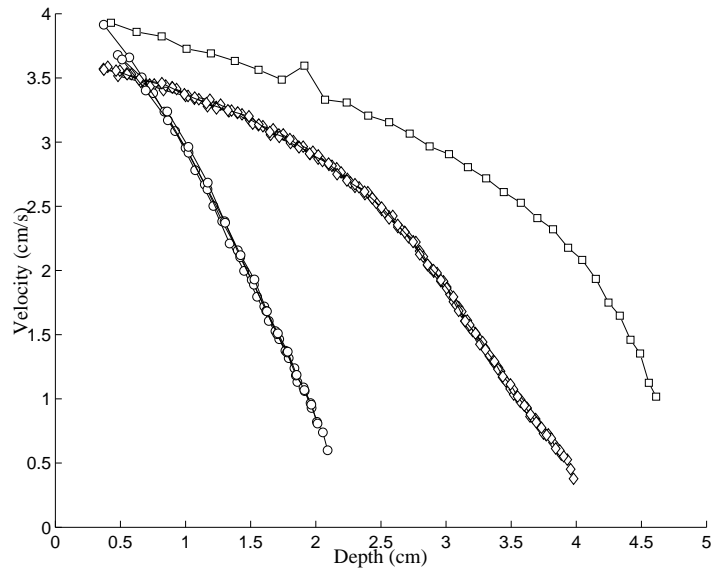


Figure 3. The evolution of the velocity of the bubbles over depth in the container is presented. \diamond - data for entrained bubbles in File 4. \circ - entrained bubble data File 3. \square - trajectory of a isolated bubble in file 4.

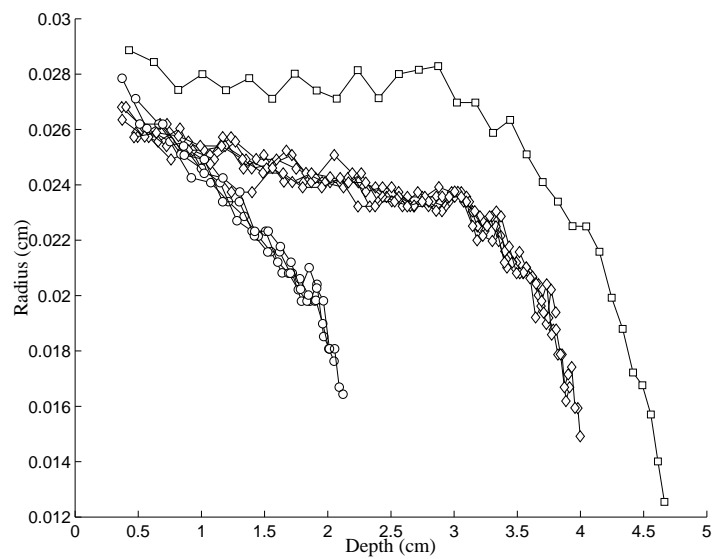


Figure 4. The evolution of the radii of the bubbles over depth in the container. \diamond - data for entrained bubbles in File 4. \circ - entrained bubble data File 3. \square - trajectory of a isolated bubble in file 4.

IV. Mathematical Model

In the present section an attempt was made to derive a model based on a force balance performed on the translating bubble. This approach is a commonly used tool in analysis of gas bubble dynamics in fluids.^{2,7,8} The main simplifications or assumptions behind this model were as follows:

- The entrained bubbles had a negligible effect on each other (an assumption that is based on Snabre et al.² who write that identical bubbles at separated by more than 1.4 times the radius can be considered non-interacting). It must be pointed out that near the nucleation point the bubbles were within this threshold and measurements at that depth are avoided. Therefore, the bubbles were considered nearly identical and were non-interacting in the interval from which the measurements are derived.
- The forces that have an appreciable effect in this model were
 - buoyancy force
 - drag force
 - inertial forces

This was an assumption that appears in other works in the subject such as Ref. 2,3,7 among others.

- The ginger ale liquid properties were approximated by the properties of water. This assumption is problematic since the purity of water has been known to have a substantial effect on the coefficient of drag which in turn has an effect on the drag force of gas bubbles in water.^{7,13} This simplification might have had an effect on the model results.
- The properties of the gas were deemed almost negligible, i.e. the density and viscosity of the gas are very small with respect to the same properties of the liquid. This was a frequent assumption that appears in many works on the subject^{2,3,5,7} as well. In this case, assuming the gas was CO₂, the ratio of the gas to liquid density is 1/500.

A. The force balance model

The following nomenclature is introduced in deriving a model for the bubble translation: $R(t)$ was the time-dependent radius of the bubble, $U(t)$ was the velocity of the bubble in its rectilinear rise and $d(t)$ was the depth of the bubble in the liquid. The constants were as follows: ρ was the density of the liquid (in this case ginger ale), ρ_g was the density of the gas, g was the gravitational acceleration constant, ν and η was the kinematic and dynamic viscosities of the liquid, respectively.

1. Drag force

For finite Reynolds number flow the following form was assumed for the time-varying drag force F_d :

$$F_d = \frac{1}{2}\rho U^2(t)\pi R^2(t)C_d$$

and was defined to act in the negative direction against overall motion induced by the buoyancy force. This particular form was derived by Moore through consideration of the boundary layer on a spherical bubble rising through liquid.⁴ In this model, the drag coefficient was deemed to be dependent on the Reynolds number with functional dependence,

$$C_d = kRe^{-\alpha}$$

with $k, \alpha > 0$ (their values were chosen in accordance to Ref. 7). Finally, Re was the dynamic Reynolds number i.e.

$$Re(t) = \frac{2R(t)U(t)}{\nu}$$

and $\nu = \eta/\rho$ was the kinematic viscosity. Ohl et al.⁷ also considered the translation of an expanding bubble via experiment and theory. The corresponding authors' experimental results agree well with their theoretical model based on the dynamic or instantaneous Reynolds number and this particular functional form is used in this work.

2. Buoyancy

The buoyancy force F_b has the well known form:

$$F_b = (\rho - \rho_g)V(t)g$$

where $V(t) = 4/3\pi R(t)^3$ is the volume of a sphere. For consistency with assumptions, it was considered that $\rho \gg \rho_g$. Consequently,

$$F_b = \rho V(t)g = \rho \frac{4\pi}{3} R(t)^3 g$$

3. Inertial force

The inertial force was derived from the so-called Kelvin impulse. Modeling the movement of the gas bubble requires an added mass term due to the displacement of the liquid as the bubble moves through the fluid. This added mass was canonically defined as half of the displaced water volume.² Therefore the impulse resulting from the bubble motion was defined as

$$I = \frac{4\pi}{3} R(t)^3 \left(\rho_g + \frac{1}{2}\rho \right) U(t)$$

to be consistent with previous assumption ($\rho_g \ll \rho$) it was held that

$$I = \frac{2\pi}{3} \rho R^3(t) U(t) \quad (1)$$

The inertial force was simply the time derivative denoted by the dot over-script of the impulse i.e. $F_i = \dot{I}$ and both the radius and velocity depend on time. Therefore:

$$F_i = 2\pi R^2(t) U(t) \dot{R} + \frac{2\pi}{3} \rho R^3(t) \dot{U} \quad (2)$$

The terms above on the right hand side above are typically referred to as the added mass terms. The resulting force balance was as follows:

$$F_i = F_b - F_d \quad (3)$$

Solving for \dot{U} it is obtained that

$$\dot{U} = 2g - \frac{3\dot{R}}{R} U - \frac{3C_d}{4R} U^2 \quad (4)$$

which is a non-linear ordinary differential equation with non-constant coefficients since the radius time derivative is non-zero in this case. The equation is a special case of the equations that appear in Ref. 7 or 13. This is the governing equation for the model of the velocity evolution over time. The equation requires an explicit formulation of the radius and its time derivatives.

B. The numerical implementation

This model can be solved numerically. In order to avoid the mechanism that produces the bubble expansion (it's functional or dynamic form is not known explicitly), a polynomial was fitted to the data for the radius taking advantage of the fact that the data from the video # 4 has reasonably similar profiles. Therefore the radius was modeled as a function of the depth which in turn depended on time through the velocity. This allowed the consideration of Equation 4 as part of a coupled set of non-linear ODE's with two unknown functions $U(t)$ and $d(t)$. The second ODE in effect was simply

$$\dot{d} = -U(t).$$

As an example of this implementation, the radius data for an entrained bubble of video # 4 was fitted with a 5-th order polynomial of d . It was considered that $d(t)$ was a function of time as well and so an approximate time dependent radius was obtained as follows:

$$R(t) \approx p_5 d^5(t) + p_4 d^4(t) + p_3 d^3(t) + p_2 d^2(t) + p_1 d(t) + p_0 \quad (5)$$

where

$$p_5 = -0.000106, p_4 = 0.000594, p_3 = -0.000400, p_2 = -0.002445, p_1 = 0.002840, \text{ and } p_0 = 0.025007,$$

The resulting disadvantage of this approach is that the velocity of the bubbles cannot be modeled in general since there are clear differences in the profile for the radius vs. depth for bubbles that originate at differing points. Although it was a simple task to fit a curve to any profile of bubble dependence on the depth, the universality of the model was greatly reduced as a result of this simplification. The advantage that resulted was that modeling results can be compared directly to the data without a detailed understanding of the mechanism behind the expansion of the bubble.

Another consideration in the model is the functional form of the drag coefficient C_d . For example in Ref. 7, the corresponding authors fitted the data to produce 2 sets values of α and k . They showed the results of two such cases:

- $\alpha_1 = .97$ and $k_1 = 107.8$
- and $\alpha_2 = .939$ and $k_2 = 76.28$.

These values resembled the steady volume case where the drag coefficient has the form

$$C_d^* = 48/Re$$

in the large Re limit. It was clear that $k_1, k_2 > 48$ and Ohl et al.⁷ wrote that this was due to the contaminants in the liquid. This most likely applied to a greater extent in the present experiment where the liquid is an amalgamation of water, ginger flavoring, sugar and other compounds. Given that Ohl et al. used purified water in their analogous experiment, the results might be improved with larger values of k .

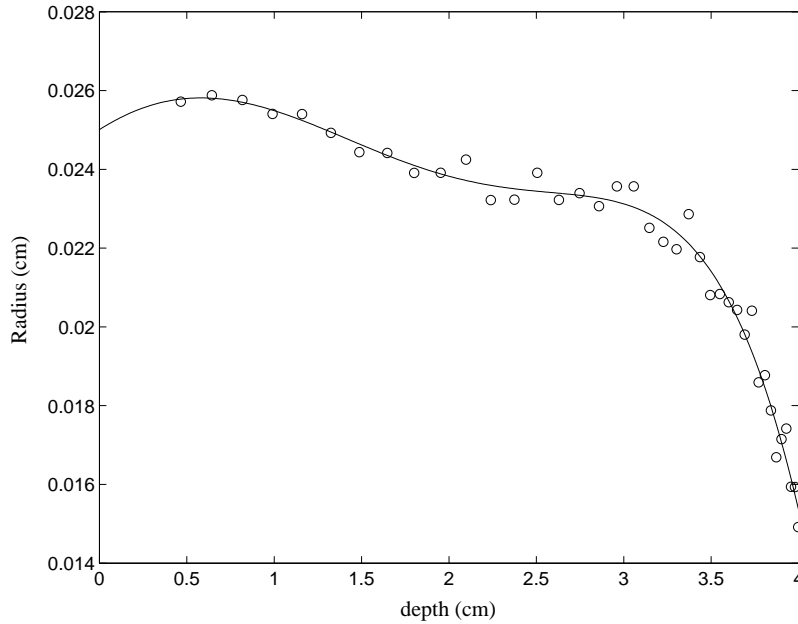


Figure 5. The 5-th degree fit for the radius as a function of depth for a bubble in data set # 4. (○) Data for radius over time for bubble in data set # 4. (—) Interpolating polynomial fit to the data.

Therefore one can formulate the following coupled system of differential equations initial value problem:

$$\begin{aligned} \dot{d} &= -U, \\ \dot{U} &= 2g - \frac{3\dot{R}(d)}{R(d)}U - \frac{3C_d}{4R(d)}U^2, \\ U(t=0) &= U_0, \quad d(t=0) = d_0. \end{aligned} \tag{6}$$

The initial data depended on the particular bubble whose velocity profile was modeled. Using an adaptive Runge-Kutta method solver for initial value problems, the numerical approximation to the solution to the full problem was obtained. The results appear in section V.

V. Discussion

A. Comparing model predictions and data

As mentioned previously, the entrained bubbles starting at the same depth behave similarly as shown in the figures for the radii and velocity. The data motivated the conclusion that the initial depth plays a large part in the dynamics of growth and velocity of the bubbles. As described in the numerical implementation of Equation 4, a polynomial was fitted in d to the empirical data for the radius profiles of the bubbles and therefore the equations can be integrated numerically using that $\dot{d} = -U$. Figure 6 was a typical result of the algorithm using the two suggested sets of values used in Ref. 7 for an entrained bubble from File # 4, i.e. It can be noted that the model did not predict the initial velocities very well. However, near the surface

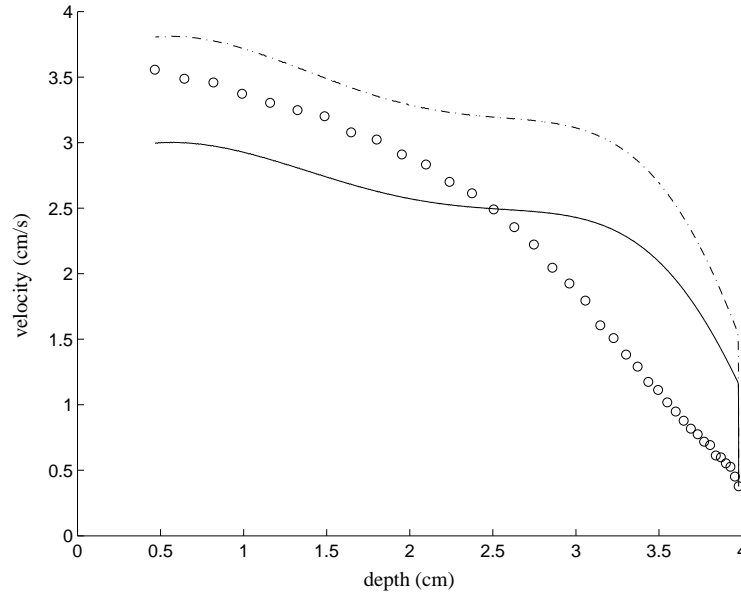


Figure 6. The comparison of the data with the model results in terms of velocity vs. depth. (–) Model prediction with $k_1 = 107.8$, and $\alpha = .97$. (---) Model result with $k_2 = 78.6$ and $\alpha_2 = .939$. (○) Data for the velocity as a function of depth.

the model did improve its prediction of the shape of the profile. Specifically for the values of k_1 and α_1 , the model predicted the final velocity to within 14% and likewise for the second case the prediction is 8.5% above the data values.

Figure 7 shows a plot of the displacement from the nucleation point versus the model prediction for the bubble considered above. One can again notice that the model predictions over-estimate the displacement initially but eventually predicts a similar shape which agreed with the earlier conclusion that the model and data velocities are closer near the surface of the container.

B. Conclusions and future considerations

It is clear that the model was over-predicting the velocity of the bubbles initially. To some extent, the model predictions improved as the motion of the bubble continued however it seems that there is something fundamental missing from this model. The model's shortcomings might be due to a variety of reasons related to the physical processes at work. The possible reasons for these defects in the model are summarized below.

1. The history force

Much work in the area considers the so-called history force which incorporates the history of the bubble as it accelerates through the liquid and generally acts against the flow of the bubble's motion similarly to the viscous drag force.¹³ Takemura and Magnaudet⁹ define that the history force results from "unsteady diffusion of vorticity from the particle surface". In general the history force has the following mathematical

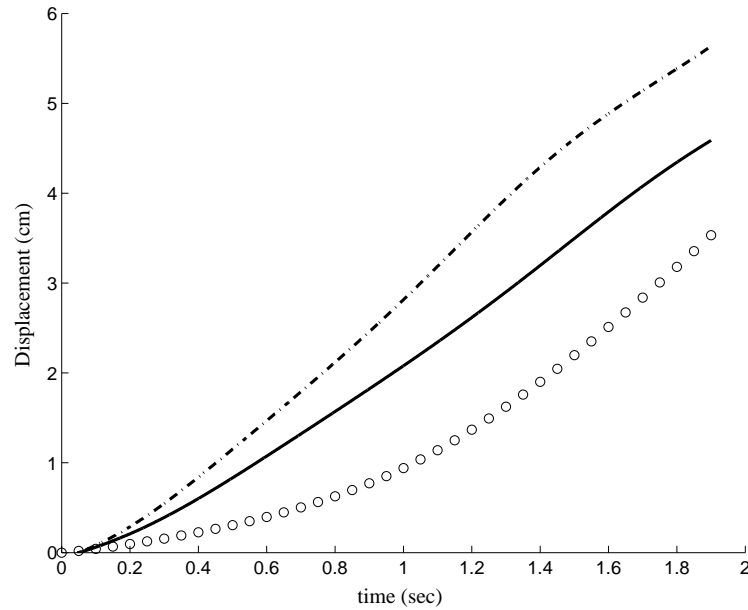


Figure 7. The comparison of the data with the model results in terms of displacement vs. time. (–) Model prediction with $k_1 = 107.8$, and $\alpha = .97$. (---) Model result with $k_2 = 78.6$ and $\alpha_2 = .939$. (○) Data for the velocity as a function of depth.

form:

$$F_H(t) = \int_{-\infty}^t K(t - \tau) \frac{d(U(\tau)R(\tau))}{d\tau} d\tau$$

It is appreciated in the literature that there exists a history force even in the absence of a translation acceleration due to the possible variation in the radius. This is apparent from the above equation in the inner derivative. The function $K(t - \tau)$ is referred to as the kernel and has different form depending on the Reynolds number regime and bubble properties. For example, Ref. 9 and Ref. 14 present history force kernels for a shrinking bubble, and a spherical bubble in finite Reynolds number flow, respectively. A natural extension of the present work is to incorporate a history force into the model. The incorporation of this force might moderate the initial accelerations of the bubbles since the history force does act against the motion of the bubble.

2. The drag force functional form

It is possible the drag force was incorrectly defined. The coefficient of drag functional form was entirely empirical in origin and loosely based on the steady-state theory. In the present model, the coefficient of drag depended on the specific choice of the parameters k and α . These values were chosen for data fitted to rising bubbles in purified water, a different circumstance than in the present work. This choice might have represented an inconsistent assumption.

In effect, Park et al.¹³ write that water contaminants tend to attach themselves to the rising gas bubbles which cause bubbles to act more like rigid particles, the result being that the outer surface of the bubble will lose its mobility. This would also have an effect on the drag force perhaps changing its nature. In this experiment, the liquid was not purified water, it was at best a solution of water, ginger flavoring and assorted other compounds. These facts perhaps might explain why the radius rate of change moderated as the bubbles reached the surface. Contaminants could have caused the increased rigidity of the surface.

3. Final conclusions

In conclusion the model was found to be wanting in several respects with regards to accuracy and also qualitative differences such as local derivatives. Also the empirical fit of the radius detracted from universality and masked the true mechanics behind the radius increase which could not be attributed solely to the

pressure gradient in the fluid. However, it was a useful exercise in extracting predictions from a very simple and intuitive force balance model.

Acknowledgments

The authors would like to thank Bob Reinking for his work in producing the data and the guidance they received throughout this process. They also thank Professor Tabor for his efforts in teaching and guidance. Finally, they thank the people who made ImageJ.

References

- ¹Yang, B., Prosperetti, A., and Takagi, S., "The transient rise of a bubble subject to shape or volume changes," *Physics of Fluids*, Vol. 15, 2003, pp. 2640–2648.
- ²Snabre, P. and Magnifotcham, F., "Formation and rise of a bubble stream in viscous liquid," *The European Physical Journal B*, Vol. 4, 1998, pp. 369–377.
- ³Moore, D., "The rise of a gas bubble in viscous liquid," *Journal of Fluid Mechanics*, Vol. 6, 1959, pp. 113–130.
- ⁴Moore, D., "The boundary layer on a spherical gas bubble," *Journal of Fluid Mechanics*, Vol. 16, 1962, pp. 161–176.
- ⁵Moore, D., "The velocity of rise of a distorted gas bubbles in a liquid of small viscosity," *Journal of Fluid Mechanics*, Vol. 23, 1965, pp. 749–766.
- ⁶Kumar, R. and Kuloor, R., "The Formation of Bubble and Drops," *Advances in Chemical Engineering*, Vol. 8, Academic Press, New York, 1970, pp. 255–386.
- ⁷Ohl, C., Tjink, A., and Prosperetti, A., "The added mass of an expanding bubble," *Journal of Fluid Mechanics*, Vol. 482, 2003, pp. 271–290.
- ⁸Magnaudet, J. and Legendre, D., "The viscous drag force on a spherical bubble with a time-dependent radius," *Physics of Fluids*, Vol. 10, 1998, pp. 550–554.
- ⁹Takemura, F. and Magnaudet, J., "The history force on a rapidly shrinking bubble rising at finite Reynolds number," *Physics of Fluids*, Vol. 16, 2004, pp. 3247–3255.
- ¹⁰Feng, Z. and Leal, L., "Nonlinear Bubble Dynamics," *Annual Review of Fluid Mechanics*, Vol. 29, 1997, pp. 201–243.
- ¹¹Kwak, H.-Y. and Patton, R. L., "Gas bubble formation in non-equilibrium water-gas solutions," *Journal of Chemical Physics*, Vol. 78, No. 9, 1983, pp. 5795–5799.
- ¹²Batchelor, G., *An Introduction to Fluid Dynamics*, Cambridge University Press, 2005.
- ¹³Park, W., Klausner, J., and Mei, R., "Unsteady forces on spherical bubbles," *Experiments in Fluids*, Vol. 19, 1995, pp. 167–172.
- ¹⁴Wei, R., Klausner, J., and Lawrence, C., "A note on the history force on a spherical bubble at finite Reynolds number," *Physics of Fluids*, Vol. 6, 1994, pp. 418–420.